Dyes and Pigments 92 (2012) 1100–1107

Contents lists available at SciVerse ScienceDirect

Dyes and Pigments

journal homepage: www.elsevier.com/locate/dyepig

NMR, multi-spectroscopic and molecular modeling approach to investigate the complexes between C.I. Acid Orange 7 and human serum albumin *in vitro*

Ximin Zhou[a,b], Qing Yang[a,b], Xiaoyun Xie[a,b], Qin Hu[a,b], Fengming Qi[a,b], Zia Ur Rahman[a,b], Xingguo Chen[a,b,c,*]

[a] *State Key Laboratory of Applied Organic Chemistry, Lanzhou University, Lanzhou 730000, China*
[b] *Department of Chemistry, Lanzhou University, Lanzhou 730000, China*
[c] *Key Laboratory of Nonferrous Metal Chemistry and Resources Utilization of Gansu Province, Lanzhou 730000, China*

ARTICLE INFO

Article history:
Received 18 March 2011
Received in revised form
15 August 2011
Accepted 18 August 2011
Available online 5 September 2011

Keywords:
C.I. Acid Orange 7 (AO7)
Human serum albumin (HSA)
Nuclear magnetic resonance (NMR)
Fourier transform infrared (FT-IR)
Three-dimensional fluorescence
Molecular modeling

ABSTRACT

In this study, the interaction between C.I. Acid Orange 7 (AO7) and human serum albumin (HSA) was firstly investigated using nuclear magnetic resonance (NMR) spectroscopy in combination with fluorescence quenching spectroscopy, three-dimensional fluorescence spectroscopy, UV–vis absorption spectroscopy, Fourier transform infrared (FT-IR) spectroscopy, circular dichroism (CD) spectroscopy and molecular modeling method *in vitro*. The results of NMR data confirmed that AO7 indeed interacted with HSA, and the hydrophobic portion of AO7 should be embedded to the hydrophobic pocket of HSA. The fluorescence quenching analysis revealed that AO7 can bind to HSA. The conformational change of HSA in the presence of AO7 was confirmed by synchronous fluorescence, three-dimensional fluorescence, UV–vis absorption, FT-IR and CD spectra. The binding distance between AO7 and tryptophan residue of HSA was calculated by the efficiency of fluorescence resonance energy transfer. Molecular modeling showed that hydrophobic force and hydrogen bonds were the major interaction between AO7 and HSA.

1. Introduction

Dyes are widely used in various products such as textiles, paints, papers, printing inks, plastics, fibers, rubbers, ceramics and food industries [1,2]. Dyestuffs are the major constituents of industrial wastewater, which is produced from these industries. In recent years, dyestuff pollution of the ecological environment has caused widely public concern. Approximately, 10,000 different dyestuffs are used to textile industry and among them, azo dyes are considered to be resistant to attack by aerobic microorganisms and not amenable to aerobic effluent treatment process [3]. C.I. Acid Orange 7 (AO7, structure shown in Fig. 1), which is generally called "Orange II", is commonly used in tanneries, paper manufacturing and textile industry in dyeing of synthetic fiber, wool and cotton [4], which is one of the most studied azo dyes in aiming decolorization of its solutions by microorganisms [5] and biodegradation [6].

Among bio-macromolecules, HSA is one of the most extensively studied soluble protein's constituents of the circulatory system, which has many important physiological and pharmacological functions [7]. Its three-dimensional structure has been determined through X-ray crystallographic measurements [8]. It is a single polypeptide chain of 585 amino acids with a largely α-helical, which consists of three homologous domains (I–III) that assemble to form a heart-shaped molecule. Each domain can be divided into two subdomains, A and B, which are formed from six and four α-helical, respectively. Its amino acid sequence contains a total of 17 disulfide bridges, one free thiol (Cys-34) and a single tryptophan (Try-214) [8]. HSA serves as a depot protein and a transport protein for many exogenous compounds [7], it can bind and carry a large number of compounds such as drugs, unesterified fatty acids, bilirubin, bile acids, metabolites, dyes, etc. [9–12]. As a result, studying of the dye–protein complex is crucial to understand the biological effect of dyes to the human body. However, until now, the mechanism of the interaction between AO7 and HSA has not been investigated in details. In this paper, AO7 is served as a model compound to construct the study method of the interaction mechanism of azo dyes and HSA.

This study was designed to research a new array on the interaction between AO7 and HSA under physiological conditions *in vitro*. In this paper, we investigated the binding mechanism between AO7 and HSA by NMR spectroscopy, fluorescence

* Corresponding author. Tel.: +86 931 8912763; fax: +86 931 8912582.
E-mail address: chenxg@lzu.edu.cn (X. Chen).

0143-7208/$ – see front matter © 2011 Elsevier Ltd. All rights reserved.
doi:10.1016/j.dyepig.2011.08.012

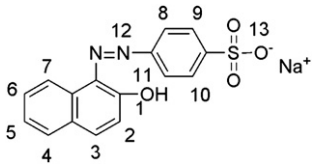

Fig. 1. The chemical structure and number systems of AO7.

quenching spectroscopy, three-dimensional fluorescence spectroscopy, UV–vis absorption spectroscopy, FT-IR spectroscopy, CD spectroscopy and molecular modeling method for the first time. AO7–HSA system was studied qualitatively and quantitatively by NMR data. The binding constants (K), number of binding sites (n) and basic thermodynamic parameters under different temperatures were calculated according to Scatchard plot and Van't Hoff equation. In addition, the synchronous fluorescence and three-dimensional fluorescence spectra were carried out to reveal the changes of tryptophan and tyrosine residues of HSA. At the same time, the alterations of the protein's secondary structure induced by the addition of AO7 were investigated by UV–vis absorption spectroscopy, FT-IR spectroscopy and CD spectroscopy. The molecular modeling study and thermodynamic analysis showed that AO7 could bind to HSA through hydrophobic force and hydrogen bonds.

2. Materials and method

2.1. Materials

AO7 and HSA (fatty acid-free $< 0.05\%$) were purchased from Sigma Chemical Company. They were used without further purification and the molecular weight of HSA was assumed to be 66,500 to calculate the molar concentrations. All HSA solutions were prepared in pH 7.40 buffer solution, and HSA stock solution (3.0×10^{-5} mol/L) was kept in the dark at 277 K. Tris (0.2 mol/L)–HCl (0.1 mol/L) buffer solution containing NaCl (0.1 mol/L) was used to keep the pH of the solution at 7.40. NaCl (1.0 mol/L) solution was used to maintain the ionic strength at 0.1. Dilutions of the HSA stock solution in Tris–HCl buffer were prepared immediately before use. The stock solution (1.0×10^{-3} mol/L) of AO7 was prepared in double distilled water. All other reagents were of analytical reagent grade and double distilled water was used throughout the experiments.

2.2. Apparatus and methods

2.2.1. NMR spectroscopy

^{1}H NMR spectra experiments were carried out on a Mercury Plus-400 spectrometer. The spectra were collected with 32,000 data points, 1200 Hz spectral width, 3.4 s acquisition, and 3 s relaxation delay [13]. The spin-lattice relaxation times (T1) were measured with an inversion recovery pulse sequence. All the NMR studies were carried out at 298 K.

2.2.2. Multi-spectroscopic technique

All the fluorescence emission spectra were recorded on a RF-5301PC Spectrofluorophotometer (Shimadzu, Japan) at 298 K, using 5/5 nm slit widths. The excitation wavelength was 295 nm, and the emission spectra were recorded in the range of 310–500 nm. Meanwhile, synchronous fluorescence spectra of HSA in the absence and presence of increasing amount of AO7 were measured under the same condition.

Fluorescence titration experiments: HSA (3.0×10^{-6} mol/L) solution was titrated manually by successive addition AO7 (1.0×10^{-3} mol/L) with trace syringes, and the range of AO7 concentration ranged from 1.67×10^{-6} to 1.17×10^{-5} mol/L. The fluorescence intensities were recorded at excitation and emission wavelength of 295 and 335 nm at four temperatures (289, 295, 303, and 310 K). The temperature of sample was kept by recycle water throughout experiment.

Three-dimensional fluorescence spectra were performed under the following conditions: the emission wavelength was recorded between 220 and 500 nm, the initial excitation wavelength was set to 220 nm with increment of 5 nm, the number of scanning curves was 27, and other scanning parameters were just the same as those of the fluorescence quenching spectra.

UV–vis absorption spectra were recorded on a TU-1810 UV–vis spectrophotometer (Beijing, China) equipped with 1.0 cm quartz cells. The wavelength range was 200–300 nm.

FT-IR measurements were carried out at room temperature on a Nicolet Nexus 670 FT-IR Spectrometer (USA) equipped with a Germanium attenuated total reflection (ATR) accessory, a DTGS KBr detector and a KBr beam splitter. All spectra were taken via the Attenuated Total Reflection (ATR) method with resolution of 4 cm^{-1} and 60 scans. Spectra of buffer solution were collected at the same condition. Next, the absorbance of buffer solution was subtracted from the spectra of sample solution to get the FT-IR difference spectra of proteins. The subtraction criterion was that the original spectrum of protein solution between 2200 and 1800 cm^{-1} was featureless [14].

CD measurements were performed using an Olis DSM 1000 (USA) automatic recording spectrophotometer in a 1 mm quartz cell at room temperature. Each spectrum represented the average of five successive scans. CD spectra were recorded in the range of 195–250 nm. The α-helical content of HSA was calculated from the molar ellipticity ($[\theta]$) at 208 nm using the following equation [15]:

$$\alpha - \text{helix}(\%) = \{(-[\theta]_{208} - 4000)/(33000 - 4000)\} \times 100 \qquad (1)$$

2.2.3. Molecular modeling method

The crystal structure of HSA in complex with R-Warfarin was taken from the Brookhaven Protein Data Bank (entry codes 1h9z). The potential of the 3D structure of HSA was assigned according to the Amber 4.0 force field with Kollman-all-atom charges. The initial structure of all the molecules was generated by molecular modeling software Sybyl 6.9 [16]. The geometries of these compounds were subsequently optimized to minimal energy using the Tripos force field with Gasteiger–Marsili charges. The FlexX program was used to build the interaction modes between AO7 and HSA. According to this kind of approach, a computational model of the target receptor was built, and partial binding parameters of AO7–HSA system were calculated through SGI FUEL workstations.

3. Results and discussion

3.1. NMR data for AO7–HSA system

Recently, NMR spectroscopy was applied for detecting the interaction between ligand and protein in solution [17]. In this paper, ^{1}H NMR spectroscopy was carried out to study how AO7 bound to HSA in D_2O. The concentration of AO7 was kept constant (3.0×10^{-3} mol/L) for obtaining the best signals of it, while the concentration of HSA was gradually increased.

It can be observed from ^{1}H NMR spectra (Fig. 2) that the proton signals were broadened and the split peaks arising from spin–spin

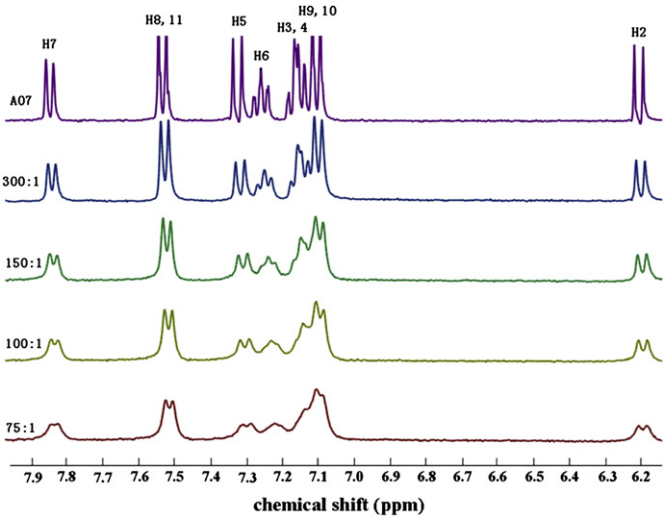

Fig. 2. ^{1}H NMR spectra of AO7 at different molar ratios of AO7 (fixed at 3.0×10^{-3} mol/L) to HSA. Assignments were presented in the topmost spectra.

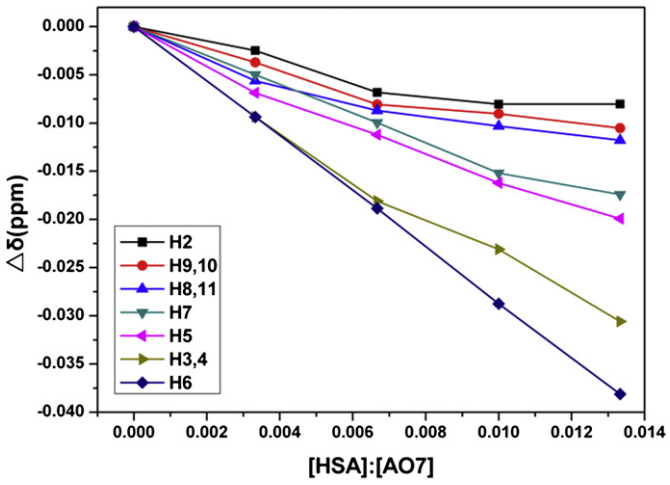

Fig. 3. Change in chemical shift ($\Delta\delta$) versus the molar ratio of HSA to AO7.

coupling overlapped into one consistently with the molar fraction of HSA in the samples. It can be concluded that AO7 underwent first-order reversible fast exchange on the site of protein [13], and these changes were caused by the molecular interaction between AO7 and HSA [18]. All the chemical shifts of ^{1}H signals moved upfield when HSA was added, which indicated that the rings of AO7 had $\pi-\pi$ stacking with aromatic residues of HSA [19]. In general, the chemical shift, as an important parameter determined by local magnetic field, is associated with the circulation electrons that surround the nucleus, and the field commonly opposes the external applied field [18]. The upfield shift of AO7 suggested that the effective field at the proton of AO7 was decreased after the interaction between AO7 and HSA. The NMR data also showed that the hydrophobic linkage of AO7 should be in the hydrophobic cavities of HSA, and its hydrophilic groups, such as hydroxyl groups, should be exposed to the hydrophilic exterior of the protein [20]. The hydroxyl group resonance could not be observed owing to fast exchange.

In addition to the qualitative examination, the interaction between AO7 and HSA was also investigated quantitatively by NMR data. The upfield shift ($\Delta\delta$) is governed by intermolecular proximity of protons to the aromatic ring and can serve to detect the different environment of protons of AO7 which bound to HSA. As shown in Fig. 3, protons near the hydroxyl group underwent limited upfield shift while protons far from it showed a significant upfield shift, indicating that they were close to the aromatic ring in the binding site. The results suggested that aromatic residues tended to stack with the portion of AO7 far from the OH group, which may be due to the repulsion between the π cloud of the aromatic ring and the electronegative oxygen.

The alterations in the spectral parameter of the free ligand protons (T1 and selective T1) depended on the affinity constant, the concentrations of ligand and protein, and the molecular weight of the ligand–protein complex. To get more insight into the interaction between AO7 and HSA, the study on T1 and selective T1 (for H2) were investigated quantitatively. As shown in Table 1, T1 and selective T1 (for H2) of AO7 decreased by the addition of HSA. For fast exchange, the observed T1 was the weight average of the bound and free AO7 [13]. So T1 of AO7 which was interacted with HSA was expected to be much lower. All the meaning of the analysis results above indicated that AO7 indeed combined with HSA.

3.2. Multi-spectroscopic techniques for AO7–HSA system

3.2.1. Fluorescence quenching spectra

Fluorescence quenching measurements were carried out to investigate the interaction between AO7 and HSA. The conformational change in HSA was evaluated by measuring the intrinsic fluorescence intensity of protein [21] in the absence and presence of AO7. Fig. 4 showed the fluorescence emission spectra of AO7–HSA system. It can be observed from Fig. 4 that the addition of AO7 caused a gradual decrease in the fluorescence emission intensity of HSA, while AO7 was almost non-fluorescent in simulative physiological condition (pH 7.40) at λ_{ex} 295 nm. At the same time, with the gradual increase in concentrations of AO7, we observed slightly dual fluorescence behavior. The fluorescence quantum yield of a tryptophan residue may be from 0.07 to 0.10 in a non-polar interior site and from 0.32 to 0.44 in a more polar near-surface, but not completely exposed, site [22]. The above phenomenon clearly indicated that the binding of AO7 to HSA changed the microenvironment of tryptophan residue from a more polar to a less polar environment and the conformational structure of HSA. At the same time, the blue shift of maximum emission wavelength from 335 nm to 330 nm also suggested a reduction in the polarity of the microenvironment [22].

3.2.2. Binding parameters and binding sites

Quenching data were analyzed to calculate the binding constants and the number of binding sites for AO7–HSA system at different temperatures using Scatchard equation [23]:

$$\frac{r}{D_f} = nK - rK \tag{2}$$

Table 1
Spin-lattice relaxation time (T1) of AO7 (Fixed at 3.0×10^{-3} mol/L) in the Absence and Presence of HSA.[a]

AO7–HSA (n_{AO7}:n_{HSA})	H7 T1 (s)	H8,11 T1 (s)	H5 T1 (s)	H6 T1 (s)	H3,4 T1 (s)	H9,10 T1 (s)	H2 T1 (s)	H2 Selective T1 (s)
AO7	1.280	1.861	1.207	1.261	1.241	1.480	1.835	1.019
300:1	1.268	1.509	1.162	1.168	1.186	1.403	1.455	0.681
200:1	1.256	1.461	1.156	1.150	1.162	1.345	1.372	0.545
150:1	1.153	1.375	1.152	1.130	1.152	1.331	1.296	0.389
100:1	1.108	1.345	1.111	1.113	1.117	1.194	1.214	0.286

[a] Spin-lattice relaxation times of different protons of AO7 were measured through inversion recovery pulse sequence.

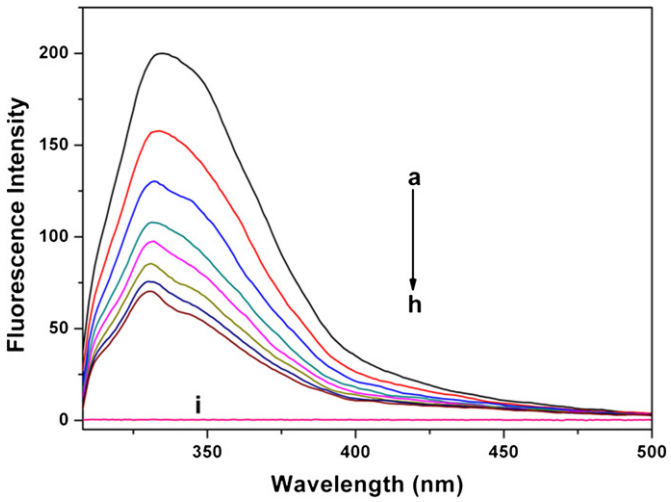

Fig. 4. The fluorescence emission spectra of AO7–HSA system. [HSA] = 3.0×10^{-6} mol/L; [AO7]/(a – h) = 0, 1.67, 3.33, 5.00, 6.67, 8.33, 10.0, 11.7×10^{-6} mol/L; (i) [AO7] = 11.7×10^{-6} mol/L; λ_{ex} = 295 nm, λ_{em} = 335 nm; pH 7.40, T = 298 K.

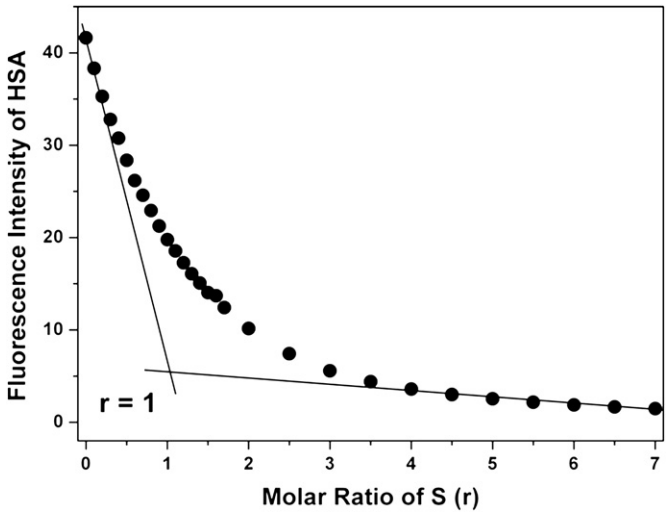

Fig. 5. Molar ratio plot for the AO7–HSA system. [HSA] = 3.0×10^{-5} mol/L; [AO7] = 0.3–21 $\times 10^{-5}$ mol/L; λ_{ex} = 295 nm, λ_{em} = 335 nm; pH 7.40.

where r is the number of moles of bound small molecules per mole of protein, D_f is the molar concentration of free small molecules, n and K are the number of binding sites and the binding constant, respectively.

The Scatchard plots were investigated at different temperatures for AO7–HSA system (figure was not shown). The linearity of the Scatchard plots indicated that AO7 bound to a single class of binding site on HSA, which was full agreement with the number of the binding site n (approximately equal to 1). The binding constants and the number of binding sites were summarized in Table 2. In this article, the binding constants obtained from Scatchard equation were applied to the discussion of binding modes.

In order to confirm how many molecules of AO7 bound to HSA, the molar ratio plot was carried out [24]. A plot of the molar fraction of AO7 versus the fluorescence intensity at 335 nm for AO7–HSA system was measured by the addition of AO7. It can be seen from Fig. 5 that the molar ratio plot generated a curve, where two straight lines drawn through initial and final points generated a crossed point, $r = 1$. The stoichiometry of the complex of AO7–HSA system was calculated based on equation:

$$m\mathrm{HSA} + n\mathrm{AO7} = \mathrm{HSA}_m\mathrm{AO7}_n \quad (3)$$

$$r = m/n$$

If $m = 1$, n should be 1. Therefore, the molar ratio plots showed that one molecules of AO7 bound to HSA, that is to say, AO7 bound to a single class of binding site on HSA. The result was consistent with the conclusion from Scatchard equation ($n = 1$).

3.2.3. Binding mode

Generally, the non-covalent interaction contributing to interaction between protein and small molecular substrates may be hydrogen bond, van der Waals force, electrostatic force, and hydrophobic interaction force, etc. [25]. The signs and magnitudes of thermodynamic parameters for binding reactions can account for the main forces contributing to protein stability. To obtain this information, the binding constants were studied at different temperatures such as 289, 295, 303, and 310 K, respectively. If the change of enthalpy change (ΔH^0) does not vary significantly over the temperature range studied, then its value and that of entropy change (ΔS^0) can be determined from Van't Hoff equation:

$$\ln K = -\frac{\Delta H^0}{RT} + \frac{\Delta S^0}{R} \quad (4)$$

where K is the binding constant at the corresponding temperature, R is the gas constant, T is absolute temperature, ΔH^0, ΔS^0 are enthalpy change, entropy change, respectively. ΔH^0 is calculated from the slope of the Van't Hoff relationship. The free energy change ΔG^0 is estimated from the equation:

$$\Delta G^0 = \Delta H^0 - T\Delta S^0 \quad (5)$$

All the results were presented in Table 2. ΔH^0 and ΔS^0 for the binding reaction between AO7 and HSA were 4.99 kJ/mol and 118.20 J/mol K, respectively, which indicated that the binding processes were entropically driven. The negative sign for ΔG^0 indicated the spontaneity of the binding of AO7 to HSA. From the point of view of water structure, positive entropy change is generally considered as a typical evidence for hydrophobic interaction, while negative enthalpy and entropy changes arise from van der Waals force and hydrogen bond formation in low dielectric media [26]. Moreover, specific electrostatic interaction between ionic species in an aqueous solution is characterized by positive ΔS^0 value and small negative ΔH^0 value. So for AO7–HSA system, hydrophobic interaction might play a major role, which was in good agreement with the information coming from molecular modeling.

Table 2
Binding parameters and thermodynamic parameters of AO7–HSA system.

Temperature (K)	K ($\times 10^5$ L/mol)	n	ΔG^0 (kJ/mol)	ΔH^0 (kJ/mol)	ΔS^0 (J/mol K)
294	1.74	0.93	−29.17	4.99	118.20
300	1.87	0.90	−29.88		
304	2.11	0.91	−30.83		
310	2.31	0.85	−31.65		

3.2.4. Effect of AO7 on the HSA conformation

3.2.4.1. Synchronous fluorescence spectra. In the synchronous fluorescence spectra, the sensitivity associated with fluorescence is maintained while offering several advantages: spectral simplification, spectral bandwidth reduction and avoidance of different perturbing effects. So the synchronous fluorescence spectroscopy is frequently used to characterize the interaction between

fluorescence probe and proteins because it can provide information about the molecular microenvironment in the vicinity of the chromophores molecules [27]. In general, the fluorescence of protein comes from the tyrosine, tryptophan, and phenylalanine residues. According to Miller [28], with large $\Delta\lambda$ ($\lambda_{em} - \lambda_{ex}$) values such as 60 nm, the synchronous fluorescence of HSA is characteristic of tryptophan residue [29]. The synchronous fluorescence spectra of HSA with adding different concentrations of AO7 were displayed in Fig. 6. It can be seen from Fig. 6, the fluorescence of tryptophan residue was quenched by AO7 with a shift of emission to a shorter wavelength from 344 to 342 nm when $\Delta\lambda$ was 60 nm. It was indicated that the conformation of tryptophan micro-region was changed by the addition of AO7 to HSA. It is reported that the maximum emission wavelength (λ_{max}) at 330–332 nm indicates that tryptophan residue is located in the non-polar region, namely, they are buried in a hydrophobic cavity of HSA; λ_{max} at 350–352 nm shows that tryptophan residue is exposed to water, namely, the hydrophobic cavity of HSA is disagglomerated. The blue shift suggested that AO7 bound to the hydrophobic cavity of HSA, which resulted in a decrease in the polarity around the tryptophan residue and the hydrophobicity was increased. The conclusion was in accordance with the results from molecular modeling and binding mode obtained by the experimental data.

3.2.4.2. Three-dimensional fluorescence spectra. The three-dimensional fluorescence spectroscopy is a newly developed fluorescence analytical technique and has become more and more popular in recent years. It can extensively reflect the fluorescence information of the protein, making investigation of the characteristic conformational change of HSA more convenient and credible [30]. Fig. 7 was the three-dimensional fluorescence spectra of HSA and AO7–HSA system, and the corresponding characteristic parameters were listed in Table 3. As shown in Fig. 7, peak a is the Rayleigh scattering peak ($\lambda_{ex} = \lambda_{em}$), and peak *b* is the second-order scattering peak ($\lambda_{em} = 2\lambda_{ex}$) [30] Because when $\lambda_{ex} = 280$ nm, the emission spectra can reveal the intrinsic fluorescence of tryptophan and tyrosine residues, as the primary fluorescence peak, peak 1 mainly reveals the spectral characteristics of tryptophan and tyrosine residues. This phenomenon can also be found in UV–vis absorption spectra (Fig. 8, curve a) following, in which there was a peak around 280 nm and this peak mainly resulted from the transition of $\pi \rightarrow \pi^*$ of aromatic amino acids in HSA. The tryptophan,

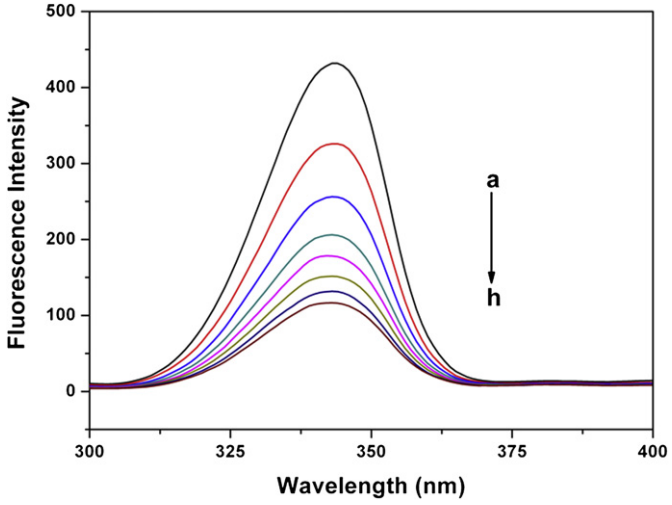

Fig. 6. Synchronous fluorescence spectra of HSA with $\Delta\lambda$ = 60 nm. [HSA] = 3.0 × 10^{-6} mol/L; [AO7]/(a – h) = 0, 1.67, 3.33, 5.00, 6.67, 8.33, 10.0, 11.7 × 10^{-6} mol/L; pH 7.40, T = 298 K.

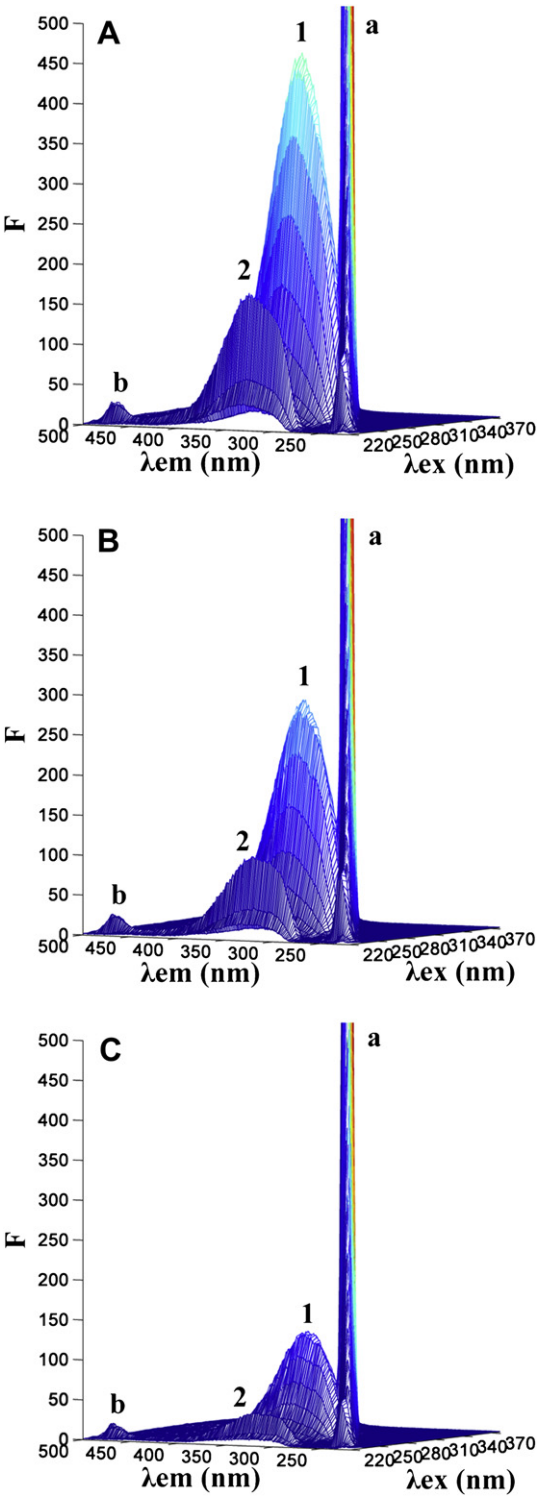

Fig. 7. The three-dimensional fluorescence spectra of free HSA (A) and AO7–HSA system (B, C). [HSA]: (A) 3.0 × 10^{-6} mol/L, (B) 3.0 × 10^{-6} mol/L, (C) 3.0 × 10^{-6} mol/L; [AO7]: (A) 0 mol/L, (B) 3.0 × 10^{-6} mol/L, (C) 12.0 × 10^{-6} mol/L; pH 7.40, T = 298 K.

tyrosine and phenylalanine residues in binding cavity of HSA have conjugated π-electron absence or π-electrons system [31]. The heterocyclic ring of AO7 can bind to the hydrophobic amino acid residues of HSA through hydrophobic forces. Besides peak 1, there is another fluorescence peak 2 which mainly exhibits the fluorescence spectral behavior of HSA's characteristic polypeptide

Table 3
Three-dimensional fluorescence spectral characteristics of HSA and AO7–HSA system.

System		Peak 1 ($\lambda_{ex}/\lambda_{em}$)	$\Delta\lambda$ (nm)	Intensity	Peak 2 ($\lambda_{ex}/\lambda_{em}$)	$\Delta\lambda$ (nm)	Intensity	Intensity ratio
HSA		285/334	49	462.453	230/335	105	170.293	2.72:1
$n_{AO7}:n_{HSA}$	1:1	285/332	47	292.688	230/332	102	104.258	2.81:1
	4:1	285/330	45	134.014	235/331	96	40.871	3.27:1

backbone structure [32]. According to Fig. 7, with adding AO7, the fluorescence intensity of peak 1 decreased, which indicated that the microenvironment of tryptophan and tyrosine residues has been changed. Peak 2 also altered similarly to peak 1 with the addition of AO7, showing that the peptide strands structure of HSA has also been altered. Analyzing from the intensity changes of peak 1 and peak 2, which decreased obviously but to different degrees (Table 3), the decrease in fluorescence intensity of the two peaks was consistent with the results of synchronous fluorescence spectra. The above phenomena were in combination with the results of synchronous fluorescence spectra, which revealed that the interaction between AO7 and HSA induced some microenvironmental and conformational change in HSA.

3.2.4.3. UV–vis absorption, FT-IR and CD spectra. In order to obtain more information on the binding of AO7 to HSA, the UV–vis absorption spectroscopy was carried out. The absorption of HSA (about 210 nm) represents the α-helical structure of HSA [33]. Fig. 8 showed the UV–vis absorption spectra of HSA in the absence and presence of AO7. It can be seen from Fig. 8, the absorbance of HSA at 211 nm decreased with the addition of AO7. At the same time, a red shift of the spectra in AO7–HSA system from 211 nm to 214 nm can also be observed. These two results clearly indicated that AO7 bound to HSA and the conformation of HSA was changed.

Further evidence of conformational change of HSA upon addition of AO7 was provided by FT-IR spectroscopy. IR spectra of proteins exhibit a number of so called amide bands, which represent different vibrations of the peptide moieties. Of all the amide bands of the proteins, amide I ranging from 1600 cm^{-1}–1700 cm^{-1} (mainly C=O) has been widely used as typical ones [34], which has a relationship with the secondary structure of the protein. Fig. 9 showed the FT-IR spectra of free HSA and difference spectra of HSA (subtracting the absorption of the AO7-free form from that of the AO7–HSA bound form). From Fig. 9 we can see that the peak position of amide I band shifted from 1641.15 to 1646.94 cm^{-1} after addition of AO7. The changes of this peak position and peak shape demonstrated that AO7 interacted with HSA and caused a change in the secondary structure of HSA.

In addition to UV–vis absorption spectroscopy and FT-IR spectroscopy, CD spectroscopy has proved to be an alternative effective method to measure the conformational transitions of a protein. Fig. 10 showed the CD spectra of HSA with various concentrations of AO7 at pH 7.40. The CD spectrum of HSA consists of two negative bands in the ultraviolet region at 208 and 222 nm, which is typical characterization of α-helix structure of protein [35]. The reasonable explanation is that the negative peaks between 208–209 nm and 222–223 nm are both due to $n \rightarrow \pi^*$ transfer for the peptide bond of α-helical [36]. The interaction between AO7 and HSA decreased the intensity of the band without any significant shift of the peaks, while, the band of CD spectra were similar in shape, indicating that the structure of HSA was also predominantly α-helix. From the above results, it was suggested that the binding of AO7 to HSA caused the change of protein secondary structure, with the loss of helical stability. The calculating results exhibited a reduction of α-helix structures from 47.29 to 46.11% at a molar ratio HSA to AO7 of 1:1.

3.2.5. The energy transfer for AO7–HSA system

Energy transfer between small molecules and proteins have been widely used to study the ligand–HSA interaction and conformational change of HSA upon binding to a ligand in the solution conditions [37]. According to the Förster non-radiative resonance energy transfer theory [38], energy transfer would happen if the following conditions are in existence: (a) the donor can produce fluorescence; (b) the fluorescence emission spectrum of the donor and the UV–vis absorption spectrum of the acceptor overlap; and (c) the distance between the donor and the acceptor is less than 8 nm [38]. The distance between the donor (tryptophan

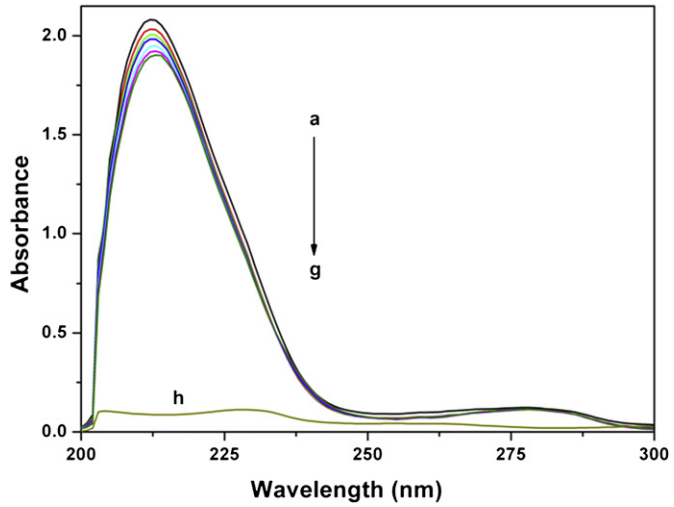

Fig. 8. UV–vis absorption spectra of AO7–HSA system. [HSA] = 3.0 × 10^{-6} mol/L; [AO7]/(a – g) = 0, 1.67, 3.33, 5.00, 6.67, 8.33, 10.0 × 10^{-6} mol/L; (h) [AO7] = 10.0 × 10^{-6} mol/L; pH 7.40, T = 298 K.

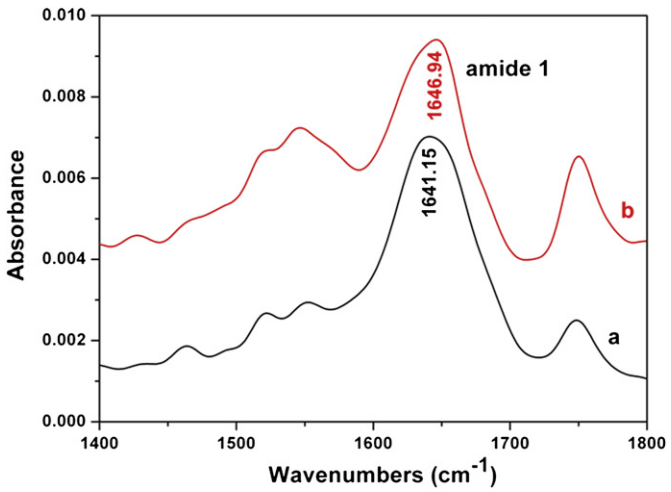

Fig. 9. FT-IR spectra of free HSA (a) and difference spectra [(HSA solution + AO7 solution) – (AO7 solution)] (b) in Tris buffer in the region of 1800–1300 cm^{-1}. [HSA] = 3.0 × 10^{-5} mol/L; [AO7] = 3.0 × 10^{-5} mol/L; pH 7.40, T = 298 K.

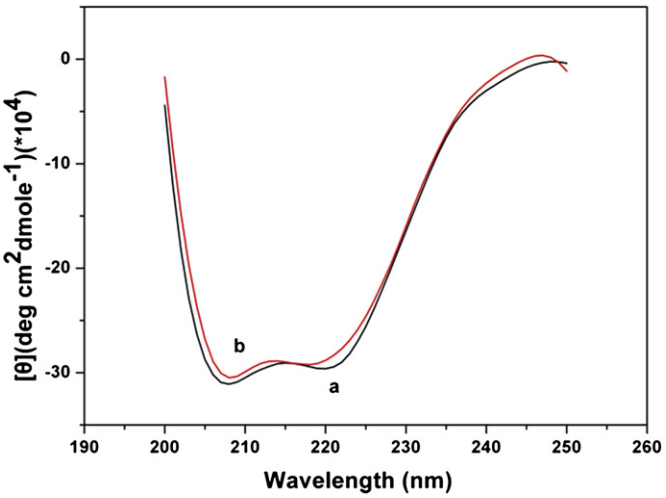

Fig. 10. CD spectra of AO7–HSA system. (a) 3.0×10^{-6} mol/L HSA; (b) 3.0×10^{-6} mol/L HSA + 3.0×10^{-6} mol/L AO7; pH 7.40, $T = 298$ K.

residue) and the acceptor (dye) can be calculated according to the theory. The efficiency of energy transfer (E) from donor to acceptor is related to the distance (R_0) in this case between HSA and AO7 can be calculated using equation:

$$E = 1 - \frac{F}{F_0} = \frac{R_0^6}{R_0^6 + r^6} \tag{6}$$

where F_0 and F are the fluorescence intensities without and with AO7, respectively, r is the binding distance between donor and receptor, and R_0 is the Förster critical distance between donor and acceptor, at which 50% of the excitation energy is transferred to acceptor and can be obtained from donor emission and acceptor absorption spectra according to equation:

$$R_0^6 = 8.79 \times 10^{-25} K^2 N^{-4} \Phi J \tag{7}$$

where K^2 is the orientation factor related to the geometry of the donor and acceptor of dipoles, N is the average refractive index of the medium in the wavelength range where spectral overlap is significant, Φ is the fluorescence quantum yield of the donor, and J is the overlap integral of the fluorescence emission spectrum of the donor and the absorption spectrum of the receptor, which could be calculated by the equation:

$$J = \frac{\sum F(\lambda)\varepsilon(\lambda)\lambda^4 \Delta\lambda}{\sum F(\lambda)\Delta\lambda} \tag{8}$$

where $F(\lambda)$ is the fluorescence intensity of the fluorescence donor when the wavelength is λ, $\varepsilon(\lambda)$ is the molar absorbance coefficient of the acceptor at the wavelength of λ.

From the overlap between the fluorescence emission spectrum of HSA and the UV–vis absorption spectrum of AO7 (figure was not shown), we could calculate the distance between AO7 and the tryptophan residue of HSA. In the present case, $K^2 = 2/3$, $\Phi = 0.14$, $N = 1.36$ [39]. According to equations (6)–(8), we calculated that $E = 0.20$ nm, $R_0 = 1.97$ nm and $r = 2.35$ nm. This data suggested that the energy transfer phenomenon between AO7 and HSA occurred efficiently.

3.3. Molecular modeling method for AO7–HSA system

The application of molecular modeling by computer methods was employed to confirm whether AO7 can bind to HSA. The principal regions of ligand binding to HSA were located in hydrophobic cavities of HSA. The best energy docking result was shown in Fig. 11. It can be seen that AO7 was located within the binding pocket of HSA, and it was important to note that the hydrophobic residues Trp-214, Leu-238, and Lys-195 were in close proximity to AO7, suggesting the existence of hydrophobic interaction between AO7 and HSA. On the other hand, there were hydrogen bonds between 12-N, 1-OH of AO7 and the residues Arg-222 of HSA, 13-O and Lys-195. For the hydrogen bond between 1-OH of AO7 and the residues Arg-222, 1-OH of AO7 was the proton-donating group, and the C=O groups of Arg-222 in HSA was the proton-accepting group. In 1-OH of AO7, the electronegativity of O atom was larger than H atom, so the electron pair was partial to O atom, resulting in the H atom was a positively charged. When AO7 bound to HSA, the hydrogen bond was produced by the C=O groups of Arg-222 because of the larger electronegativity of O atom in C=O.

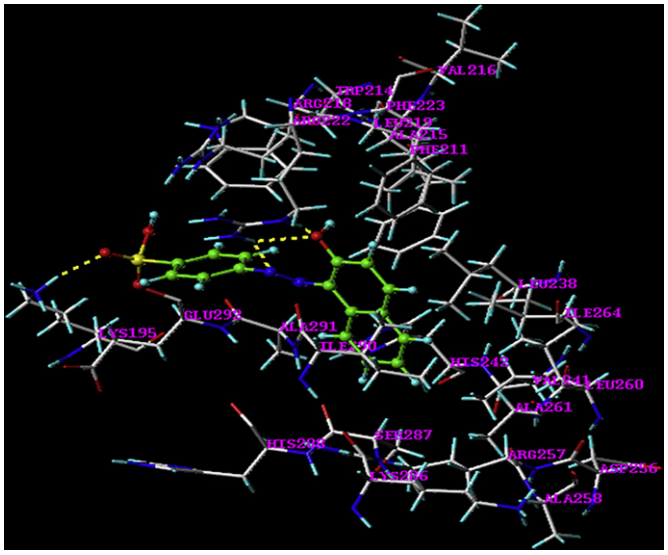

Fig. 11. The interaction model between AO7 and HSA. Only residues around 6.5 Å of the ligand are displayed. The residues of HSA are represented using the line model and the AO7 structure is represented using a ball and stick model. The hydrogen bonds between AO7 and HSA are represented by dashed line. (For interpretation of the references to color in this figure legend, the reader is referred to the web version of the article.)

The results indicated that the formation of hydrogen bonds decreased the hydrophilicity and increased the hydrophobicity to stabilize AO7–HSA system. Therefore, the results obtained from molecular modeling method indicated that AO7 can bind to HSA, and the interaction between them was dominated by hydrophobic force and hydrogen bonds. In addition, the calculated binding Gibbs free energy (ΔG^0) was −25.82 kJ/mol, which was not extremely close to the experimental data (−29.17 kJ/mol) in some degree. A possible explanation may be that the X-ray structure of the protein from crystals differs from that of the aqueous system used in this study.

4. Conclusions

In this work, we firstly investigated the interaction between AO7 and HSA by NMR spectroscopy, multi-spectroscopic technique consisting of fluorescence quenching spectroscopy, three-dimensional fluorescence spectroscopy, UV–vis absorption spectroscopy, FT-IR spectroscopy, CD spectroscopy and molecular modeling method. It was shown that the dye–protein interaction can be efficiently detected using this novel NMR spectroscopy. The experimental results suggested that AO7 can bind to HSA, and the

binding of AO7 to HSA induced a conformational change of HSA. The binding distance (r) between AO7 and Trp-214 of HSA was calculated to be 2.35 nm. According to the molecular modeling study, the binding site was located within the hydrophobic pocket of HSA, and AO7 could bind to HSA through hydrophobic force and hydrogen bonds.

Acknowledgements

We are grateful for financial support from the National Natural Science Foundation of China (No. 20875040, J0730425).

References

[1] Visinescu D, Paraschiv C, Ianculescu A, Jurca B, Vasile B, Carp O. The environmentally benign synthesis of nanosized CoxZn1xAl2O4 blue pigments. Dyes Pigm 2010;87:125–31.
[2] Vishnu VS, George G, Divya V, Reddy MLP. Synthesis and characterization of new environmentally benign tantalum-doped Ce0.8Zr0.2O2 yellow pigments: applications in coloring of plastics. Dyes Pigm 2009;82:53–7.
[3] Ong SA, Toorisaka E, Hirata M, Hano T. Granular activated carbon-biofilm configured sequencing batch reactor treatment of C.I. Acid Orange 7. Dyes Pigm 2008;76:142–6.
[4] Elizalde-González MP, Hernández-Montoya V. Removal of acid orange 7 by guava seed carbon: a four parameter optimization study. J Hazard Mater 2009; 168:515–22.
[5] Forgacs E, Cserháti T, Oros G. Removal of synthetic dyes from wastewaters: a review. Environ Int 2004;30:953–71.
[6] van der Zee FP, Villaverde S. Combined anaerobic-aerobic treatment of azo dyes – a short review of bioreactor studies. Water Res 2005;39:1425–40.
[7] Xiao JB, Chen LS, Yang F, Liu CX, Bai YL. Green, yellow and red emitting CdTe QDs decreased the affinities of apigenin and luteolin for human serum albumin in vitro. J Hazard Mater 2010;182:696–703.
[8] He JX, Carter DC. Atomic structure and chemistry of human serum albumin. Nature 1992;358:209–15.
[9] Kragh-Hansen U. Molecular aspect of ligand binding to serum albumin. Pharmacol Rev 1981;33:17–53.
[10] Waheed AA, Sridhar Rao K, Gupta PD. Mechanism of dye binding in the protein assay using eosin dyes. Anal Biochem 2000;287:73–9.
[11] Tang JH, Wang WP, Luan F, Chen XG. Binding of the bioactive compound 5,7,4′-trihydroxy-6,3′,5′-trimethoxyflavone to human serum albumin. Int J Biol Macromol 2005;37:85–91.
[12] Yue YY, Chen XG, Qin J, Yao XJ. A study of the binding of C.I. Direct Yellow 9 to human serum albumin using optical spectroscopy and molecular modeling. Dyes Pigm 2008;79:176–82.
[13] Wu TQ, Wu Q, Guan SY, Su HX, Cai ZJ. Binding of the environmental pollutant naphthol to bovine serum albumin. Biomacromolecules 2007;8:1899–906.
[14] Dong AC, Huang P, Caughey WS. Protein secondary structures in water from second-derivative amide I infrared spectra. Biochemistry 1990;29:3303–8.
[15] Khan AM, Muzammil S, Musarrat J. Differential binding of tetracyclines with serum albumin and induced structural alterations in drug-bound protein. Int J Biol Macromol 2002;30:243–9.
[16] Morris G. SYBYL software, version 6.9. St. Louis: Tripos Associates Inc; 2002.
[17] Arac D, Murphy T, Rizo J. Facile detection of protein–protein interactions by one-dimensional NMR spectroscopy. Biochemistry 2003;42:2774–80.
[18] Ji ZS, Yuan HZ, Liu ML, Hu JM. ^{1}H-NMR study of the effect of acetonitrile on the interaction of ibuprofen with human serum albumin. J Pharm Biomed Anal 2002;30:151–9.
[19] Sun H, Ye KQ, Wang CY, Qi HY, Li F, Wang Y. The $\pi-\pi$ stacked geometries and association thermodynamics of quinacridone derivatives studied by ^{1}H NMR. J Phys Chem A 2006;110:10750–6.
[20] Jiang YL. Design, synthesis and spectroscopic studies of resveratrol aliphatic acid ligands of human serum albumin. Bioorg Med Chem 2008;16:6406–14.
[21] Yuan T, Weljie AM, Vogel HJ. Tryptophan fluorescence quenching by methionine and selenomethionine residues of calmodulin: orientation of peptide and protein binding. Biochemistry 1998;37:3187–95.
[22] MacManus-Spencer LA, Tse ML, Hebert PC, Bischel HN, Luthy RG. Binding of perfluorocarboxylates to serum albumin: a comparison of analytical methods. Anal Chem 2010;82:974–81.
[23] Scatchard G. The attractions of protein for small molecules and ions. Ann N Y Acad Sci 1949;51:660–73.
[24] Gonzalez-Gaitano G, Sainz-Rozas PR, Isasi JR, Guerrero-Martinez A, Tardajos G. Site-specific interaction between 2-dibenzofuran carboxylate and β- and γ-cyclodextrins determined by intermolecular NOE and molecular modeling. J Phys Chem B 2004;108:14154–62.
[25] Jiang CQ, Gao MX, Meng XZ. Study of the interaction between daunorubicin and human serum albumin, and the determination of daunorubicin in blood serum samples. Spectrochim Acta A 2003;59:1605–10.
[26] Ross PD, Subramanian S. Thermodynamics of protein association reactions: forces contributing to stability. Biochem 1981;20:3096–102.
[27] Gong AQ, Zhu XS, Hu YY, Yu SH. A fluorescence spectroscopic study of the interaction between epristeride and bovin serum albumine and its analytical application. Talanta 2007;73:668–73.
[28] Miller JN. Recent advances in molecular luminescence analysis. Proc Analyt Div Chem Soc 1979;16:203–8.
[29] Wang YP, Wei YL, Dong C. Study on the interaction of 3,3-bis (4-hydroxy-1-naphthyl)-phthalide with bovine serum albumin by fluorescence spectroscopy. J Photochem Photobiol A 2006;177:6–11.
[30] Zhang YZ, Chen XX, Dai J, Zhang XP, Liu YX, Liu Y. Spectroscopic studies on the interaction of lanthanum(III) 2-oxo-propionic acid salicyloyl hydrazone complex with bovine serum albumin. Luminescence 2008;23:150–6.
[31] Kang J, Liu Y, Xie MX, Li S, Jiang M, Wang YD. Interactions of human serum albumin with chlorogenic acid and ferulic acid. Biochim Biophys Acta 2004; 1674:205–14.
[32] Wang YQ, Tang BP, Zhang HM, Zhou QH, Zhang GC. Studies on the interaction between imidacloprid and human serum albumin: spectroscopic approach. J Photochem Photobiol B 2009;94:183–90.
[33] Wang YL, Wang HF. Interaction of bovine albumin with benzoate. Univ Pekinensia (Sci Nat) 2002;38:159–63.
[34] Sirotkin VA, Zinatullin AN, Solomonov BN, Faizullin DA, Fedotov VD. Calorimetric and Fourier transform infrared spectroscopic study of solid proteins immersed in low water organic solvents. Biochim Biophys Acta 2001;1547: 359–69.
[35] Trynda-Lemiesz L, Karaczyn A, Keppler BK, Koztowski H. Studies on the interactions between human serum albumin and trans-indazolium (bisindazole) tetrachlororuthenate(III). J Inorg Biochem 2000;78:341–6.
[36] Yang P, Gao F. The principle of bioinorganic chemistry. Beijing: Science Press; 2002.
[37] Hu YJ, Liu Y, Wang JB. Study of the interaction between monoammonium glycyrrhizinate and bovine serum albumin. J Pharm Biomed Anal 2004;36: 915–9.
[38] Förster T, Sinanoglu O. Modern quantum chemistry. 3rd ed. New York: Academic; 1996.
[39] Epps DE, Raub TJ, Caiolfa V, Chiari A, Zamai M. Evaluating the binding selectivity of transthyretin amyloid fibril inhibitors in blood plasma. J Pharm Pharmacol 1998;51:41–8.